Journal of Materials Chemistry C

ROYAL SOCIETY OF CHEMISTRY

PAPER

View Article Online
View Journal

Cite this: DOI: 10.1039/d6tc00689b

New D–π–A dyes based on indolo[3,2,1-*jk*]-carbazole and thienopyrrolo[3,2,1-*jk*]carbazole for application in dye-sensitized solar cells

Grażyna Szafraniec-Gorol, *[a] Pawel Gnida, [b] Sonia Kotowicz, [a] Pawel Czulkin [c] and Ewa Schab-Balcerzak [ab]

Received 4th March 2026,
Accepted 1st May 2026

DOI: 10.1039/d6tc00689b

rsc.li/materials-c

Six new D–π–A type molecules were designed, synthesized, and investigated. The donor moieties were rigid, tripod-shaped polycyclic heteroaromatic indolo[3,2,1-*jk*]carbazole (ICz) and thieno[2′,3′:4,5]-pyrrolo[3,2,1-*jk*]carbazole (TPCz) skeletons, while the acceptor groups were cyanoacrylic acid and rhodanine-3-acetic acid, and the linkers were phenyl, thiophene, and an acetylene bridge. TPCz is a stronger donor than ICz, which destabilises the HOMO in the molecules and lowers the energy band gap. The optical and electrochemical properties were thoroughly analysed by comparing experimental data with DFT and TD-DFT calculations. The potential of the synthesized compounds for photovoltaic applications was investigated in dye-sensitized solar cells. It was found that the device sensitized with the TPCz molecule containing a cyanoacrylic acid unit exhibited the best performance compared to the others; however, the power conversion efficiency (PCE) was low, 1.31%. This molecule appears to act as a complementary sensitizer to the commercial N719 dye. Therefore, additional device engineering strategies were implemented, including co-sensitization with N719, incorporation of a co-adsorbent (chenodeoxycholic acid), introduction of a blocking layer, and operation under reduced illumination conditions. These modifications resulted in a significant enhancement of PCE, reaching 12.30% under reduced illumination (10 mW cm^{-2}).

Introduction

As the world's population grows and industries evolve, the demand for electricity continues to increase. To meet the needs of current and future generations while minimising the negative impact on the climate, clean and renewable energy sources are increasingly being adopted. One promising solution that addresses these challenges is dye-sensitized solar cells (DSSCs). In recent years, the use of metal-free organic sensitizers (dyes) has increased rapidly due to their lower production costs and reduced environmental impact compared to Ru-based dyes.[1,2] Organic dyes offer several advantages, including broad absorption in the visible region, high molar extinction coefficients, structural tunability, relatively low fabrication costs, and straightforward synthesis and purification. The sensitizer is a crucial component of the solar cell, and its molecular design fundamentally determines device performance. The dye accumulates solar radiation and converts photons into electrons *via* a push–pull process. Electrons are transferred from the donor fragment (D) through the π-spacer to the acceptor fragment (A). Current research focuses primarily on D–π–A, D–D–π–A, or D–π–D–π–A dye structures.[3,4] Commonly investigated acceptor groups include cyanoacrylic acid,[3–8] rhodanine-3-acetic acid,[4,7] and carboxylic acid,[9] with particular attention devoted to their influence on dye adsorption onto the TiO_2 surface, electron injection efficiency, and long-term device stability. Appropriate π-spacers can improve device performance in several ways, including broadening the absorption spectrum, improving intramolecular charge transfer (ICT), or optimising molecular aggregation. Frequently employed linkers include phenyl,[3,5,6,8] thiophene,[3,6] furan,[3] or other heteroarenes. Derivatives of triphenylamine (TPA),[10] carbazole (cb),[4,5,7,11–13] phenothiazine (PTZ),[5,14–18] and indole[3,19,20]are the most commonly used donor units. More recently, polycyclic heteroaromatic (PHA) molecules containing nitrogen and sulfur atoms have emerged as promising donor motifs in DSSCs.[3] The presence of a heteroaromatic core within a rigid, conjugated scaffold can broaden absorption, facilitate intermolecular charge transfer and prevent charge recombination. Increased molecular

[a] *Institute of Chemistry, University of Silesia, 9 Szkolna Street, 40-006 Katowice, Poland. E-mail: grazyna.szafraniec-gorol@us.edu.pl*
[b] *Centre of Polymer and Carbon Materials, Polish Academy of Sciences, 34 M. Curie-Sklodowska Street, 41-819 Zabrze, Poland*
[c] *Faculty of Chemistry, Silesian University of Technology, 9 Strzody, Gliwice 44-100, Poland*

rigidity is generally beneficial for achieving higher J_{sc} values, as it enhances electron delocalisation and can reduce non-radiative energy losses. Moreover, the introduction of stronger donor motifs with dual electron-donating centers can raise the HOMO energy level and enhance ICT and light-harvesting ability, thereby contributing to improved J_{sc}.[1,3,9]

One such PHA system that has attracted significant attention in recent years in the field of organic electronics is indolo[3,2,1-*jk*]carbazole (ICz).[6,9,12,21–31] In a flat ICz structure, the availability of the nitrogen atom's free electron pair can be adjusted by attaching substituents of different electron strengths to the core. Consequently, its donor–acceptor strength can be readily tuned.[32] This enables precise modulation of its charge-transfer (CT) characteristics, which, in turn, can influence the emission wavelength and enhance the luminescence quantum yield. Such controllable optoelectronic properties are crucial for the development of advanced electronic devices. ICz derivatives have been investigated in DSSCs,[6,9,19,20] OLEDs,[22,28–30,33–36] TADF emitters,[31,37] and many others.

To our knowledge, few DSSCs with ICz-based dyes have been developed. Luo *et al.* obtained and tested the dyes with ICz as the donor, phenyl and thiophene as the π-linkers, and cyanoacrylic acid as the acceptor. The best cell, which had thiophene as a π-spacer, achieved a power conversion efficiency (PCE) of 3.68% with a V_{oc} of 0.66 V.[6]

On the other hand, Cao *et al.* developed DSSCs with 2,5-di-*tert*-butylindolo[3,2,1-*jk*]carbazole as the donor moiety, bithiophene derivatives as the π-spacers, and cyanoacrylic acid as the anchoring group. The cells' efficiency was improved by using a co-adsorbent, chenodeoxycholic acid (CDCA), whose concentration significantly affected the cells' photovoltaic properties. The best power conversion efficiency of DSSCs using D–π–A dyes was 4.66%.[21]

Recently, Al-Furaiji *et al.* synthesised two D–π–A dyes, where the donor fragment was ICz, the π-bridges were highly conjugated dithieno[2,3]pyridine derivatives, and the anchoring groups were squaraine-indoline-5-carboxylic acid. The dyes exhibited very wide absorption ranges. A DSSC based on one of these dyes exhibited a power conversion efficiency of 8.5%. Additionally, a tandem dye cell with N719 achieved an impressive efficiency of 13.55%.[9]

In our previous work, the impact of the thickness of the TiO_2 blocking layer on DSSC performance based on D–π–D–A architecture metal-free organic dyes and commercial N719 has been investigated. In our dye, the peripheral donor was ICz, the central donor was 10-octylphenothiazine and the anchoring group was cyanoacrylic acid. A DSSC based on a free dye exhibited a PCE of 3.7%. However, using a dye as a co-sensitizer in a tandem DSSC enabled the N719 loading to be significantly reduced while maintaining a PCE of 8%.[22]

The success of the dyes used in DSSCs depends on two things: efficient charge transfer from the donor to the acceptor and sufficient charge separation within the molecule. These requirements can be fulfilled by ensuring a high degree of coplanarity and extended π-conjugation across the molecular framework. Therefore, the aim in dye structures is to achieve the smallest possible dihedral angle between fragments. However, highly planar structures are prone to aggregation on the semiconductor surface, which adversely affects the photovoltaic parameters of the cell. This can be prevented by adding a co-adsorbent, such as chenodeoxycholic acid (CDCA).[38] In our study, we aimed to investigate the polycyclic heteroaromatic hydrocarbons – the well-known ICz and thieno[2′,3′:4,5]pyrrolo[3,2,1-*jk*]carbazole (TPCz).

The synthesis and optical and electrochemical properties of TPCz were first published by Bader *et al.*[39] The donor strength of this skeleton in relation to ICz is enhanced by replacing the phenyl ring with a thiophene ring. TPCz exhibits a flat molecular geometry and destabilises the HOMO and stabilises the LUMO level, highlighting its strong potential as a donor component in donor–acceptor architectures. To the best of our knowledge, this is the first report describing the application of TPCz as a donor building block in D–π–A-type functional organic materials.

Inspired by such findings, we designed and synthesised six novel D–π–A type dyes, denoted as **ICz-A**, **ICz-B** and **TPCz-A**–**TPCz-D**. The donor fragments are tripod-flat fused PHA: indolo[3,2,1-*jk*]carbazole (ICz) and thieno[2′,3′:4,5]pyrrolo[3,2,1-j*k*]carbazole (TPCz). The thermal, optical, and electrochemical properties were examined and correlated with DFT and TD-DFT calculations. The synthesized compounds were evaluated as sensitizers in third-generation photovoltaic (PV) devices, namely, dye-sensitized solar cells (DSSCs), in order to assess their photovoltaic performance under reduced irradiance conditions. Owing to their distinctive optoelectronic properties, DSSCs are considered promising candidates for efficient energy conversion in low-irradiance environments.[10,40,41]

Results and discussion

Synthesis, structural characterization and thermal properties

Our previous studies have consistently demonstrated the applicability of ICz both as a sensitizer in DSSCs and as a light-emitting material.[16,28,29] Inspired by Bader's work[39] on enhancing the donor strength of TPCz, we designed a series of six D–π–A dyes. In all structures, the donor unit consists of a planar, fused-ring scaffold connected to the acceptor through a simple π-spacer (phenyl or thiophene). Five of the dyes incorporate a phenyl π-linker, with **TPCz-D** being the only exception. An additional acetylene bridge is introduced into four derivatives: **ICz-A**, **ICz-B**, **TPCz-A** and **TPCz-B**. The –C≡C– linkage extends π-conjugation while simultaneously enhancing the intramolecular charge transfer (ICT) characteristics. Cyanoacrylic acid and rhodanine-3-acetic acid were employed as electron-withdrawing/anchoring groups. The chemical structures of the designed, synthesized, and investigated D–π–A compounds are presented in Fig. 1. The multistep synthesis procedure for the aforementioned dyes is outlined in Scheme S1 in the supplementary information (SI). The first stage involved the preparation of the donor cores (ICz and TPCz)

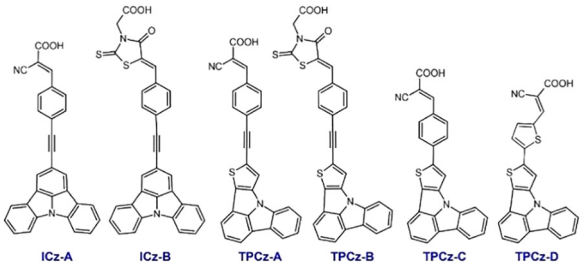

Fig. 1 The structures of the obtained dyes (**ICz-A**– **TPCz-D**).

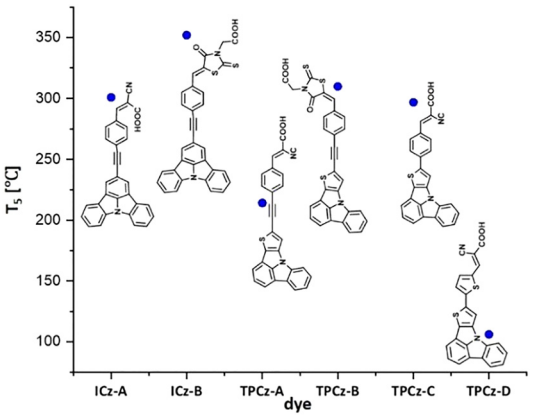

Fig. 2 Temperatures corresponding to 5% weight loss (T_5) determined *via* TGA for the investigated dyes.

according to our previously reported procedure for ICz[29] and literature methods for TPCz.[39] Monosubstituted halogen intermediates were subsequently obtained using NIS as an iodinating agent, yielding 2-iodoindolo[3,2,1-*jk*]carbazole (ICz-I) and 5-iodo-thieno[2′,3′:4,5]pyrrolo[3,2,1-*jk*]carbazole (TPCz-I). In the subsequent step, Sonogashira and Suzuki–Miyaura cross-coupling reactions were carried out using [$Pd(PPh_3)_4$] as the catalyst. For the Sonogashira reactions, CuI was used as a co-catalyst, with NEt_3/THF as the solvent, and the reactions were conducted at 70 °C for 24 h. In the Suzuki–Miyaura reactions, a 2M sodium carbonate solution served as the base in a toluene/ethanol solvent system; these reactions were performed at 90 °C for 24 h. The target compounds were obtained in yields of up to 90%. The final dyes (Fig. 1) were obtained *via* Knoevenagel condensation. For **ICz-A**, **TPCz-A**, **TPCz-C**, and **TPCz-D**, cyanoacetic acid (11 equiv.) was used, whereas rhodanine-3-acetic acid (4 equiv.) was used for **ICz-B** and **TPCz-B**. The reactions were carried out in $CHCl_3$/MeCN or EtOH at 80–90 °C for 24 h, affording the desired products in yields ranging from 23% to 86%. The chemical structures and purities of the dyes were confirmed by ^1H and ^{13}C NMR and high-resolution mass spectrometry.

Organic dyes employed in DSSCs must exhibit sufficient thermal stability to ensure reliable operation within the typical device temperature range (25–80 °C). To evaluate the thermal stability of synthesized compounds, thermogravimetric analysis (TGA) was performed under a nitrogen atmosphere (see the SI, Fig. S1). The temperature corresponding to 5 (T_5) and 10% (T_{10}) weight loss and maximum decomposition rate temperature (T_{max}) from the differential curve (DTG) and char residue at 700 °C are presented in Table S1 in the SI. All dyes exhibit relatively high char residues at 700 °C, ranging from 48% to 73%. The T_5 values range from 106 to 352 °C (see Fig. 2), and major decomposition processes occur in the 215–382 °C range for all dyes. With the exception of **TPCz-D**, no significant mass loss is observed below 214 °C for most dyes. Among the investigated compounds, **ICz-B** displays the highest thermal stability. Overall, dyes incorporating the ICz core exhibit slightly higher thermal stability than their **TPCz**-Based analogues. A comparison of **TPCz-A** and **TPCz-C** indicates that the introduction of an additional acetylene linker reduces the thermal stability of the TPCz derivatives, as reflected by lower T_5 and T_{max} values (Table S1 in the SI and Fig. 2). Moreover, **TPCz-D** is the least thermally stable compound, suggesting that incorporation of a thiophene bridge significantly weakens the structural integrity of the dye. Such reduced thermal stability may adversely affect the long-term operational stability of DSSCs sensitized with **TPCz-D**. Nevertheless, the thermal stability of the remaining dyes exceeds that of our previously reported donor–acceptor dye based on ICz-phenothiazine derivatives[16] and is comparable to that of other ICz-containing dyes reported in the literature,[9] supporting their applicability as DSSC sensitizers.

Theoretical calculations

For a more in-depth analysis of the optical and electrical properties, as well as explanations of the results of photovoltaic behaviour of prepared dyes **ICz-A**–**TPCz-D**, the quantum chemical calculations based on density functional theory (DFT) and time-dependent-density functional theory (TD-DFT) were carried out using the Gaussian 16 program[42] and B3LYP and CAM-B3LYP exchange–correlation functionals were employed. The LANL2DZ basis set was used to model the titanium atoms in calculations involving $(TiO_2)_9$ clusters, while other atoms were modelled using the 6-31G(d,p) basis set. To account for solvation effects in dichloromethane, all calculations were conducted using the polarizable continuum model (PCM).[43] Table 1 presents the optimised geometries, HOMO and LUMO distributions, their energies, and the percentage contributions of the different molecular fragments (donor core, phenyl/thiophene ring, acetylene linker, and anchoring group) calculated at the B3LYP level for **ICz-A**–**TPCz-D**. The HOMOs of all dyes are predominantly localized on the donor core (ICz or TPCz). In **ICz-A**, **ICz-B**, **TPCz-A**, and **TPCz-B**, approximately 15% of HOMO density is distributed over the ethynyl bridge, while a further 13% is localized on the phenyl ring. For **ICz-B** and **TPCz-B**, which incorporate rhodanine-3-acetic acid as the anchoring group, about 12% of the HOMO density resides on the rhodanine ring, whereas no significant contribution is observed from the terminal carboxylic acid group. In the dyes lacking an additional acetylene linker (**TPCz-C** and **TPCz-D**), 16% and 22% of HOMO density are localized on the phenyl and thiophene linkers, respectively. The LUMOs are mainly localized on

Table 1 Optimised structures (B3LYP/6-311G(d,p), DCM) of **ICz-A–TPCz-D**, including HOMO and LUMO contour plots (isovalue = 0.025), frontier orbital energies, and percentage contributions of individual molecular fragments (core, ring, acetylene bridge, and anchoring group) to the frontier molecular orbitals

Dye	% HOMO	HOMO [eV]	LUMO [eV]	% LUMO	ΔE [eV]
ICz-A	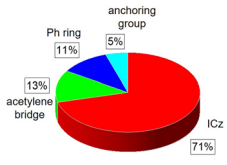	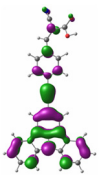 −5.93	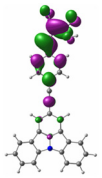 −3.18	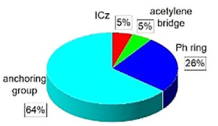	2.75
ICz-B	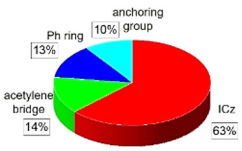	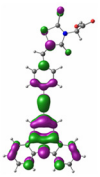 −5.88	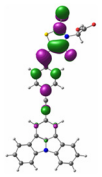 −3.28	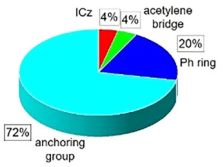	2.6
TPCz-A		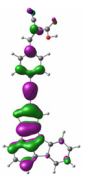 −5.77	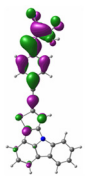 −3.13	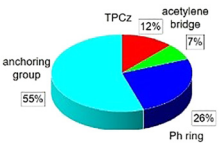	2.64
TPCz-B	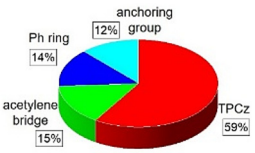	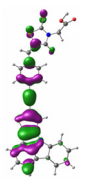 −5.70	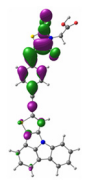 −3.18	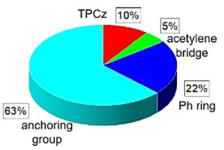	2.52
TPCz-C	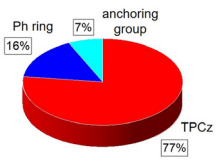	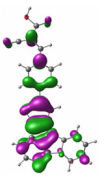 −5.95	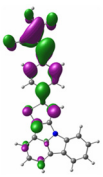 −3.22	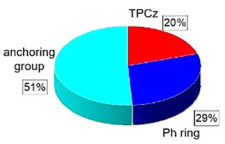	2.73
TPCz-D	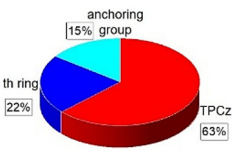	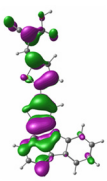 −5.94	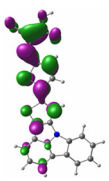 −3.39	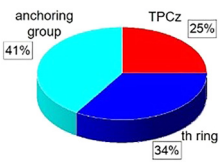	2.55

the anchoring acceptor groups, which is favorable for electron injection from the photoexcited dye into the conduction band of TiO_2 upon adsorption onto the semiconductor surface. In addition, approximately 20–34% of the LUMO density extends onto the adjacent aromatic π-spacer (phenyl or thiophene ring). This frontier molecular orbital (FMO) distribution suggests that, upon photoexcitation, charge transfer proceeds from the donor-centered HOMO (localized on ICz or TPCz) toward the acceptor-centered LUMO (localized on the anchoring group), through the conjugated π-bridges (acetylene and/or aromatic linkers), thereby promoting electron injection into TiO_2. The percentage contributions of the individual molecular fragments to the HOMO and LUMO, as obtained from DFT calculations, are very similar for both functionals (B3LYP and CAM-B3LYP).

However, as discussed below, the trends in the orbital energies and the HOMO–LUMO gaps calculated at the B3LYP level are in closer agreement with electrochemically estimated values derived from CV measurements (Table 4) than those obtained using CAM-B3LYP.

An energy-level diagram illustrating the calculated FMO energies for **ICz-A–TPCz-D** is shown in Fig. S2 in the SI. Analysis of the FMO levels reveals that the HOMO energies of all dyes are

located in the range of approximately −5.7 to −5.95 eV, substantially below the redox potential of the I^-/I_3^- couple (−4.8 eV). This energetic alignment is expected to facilitate dye regeneration and may reduce the likelihood of charge recombination between the oxidized dye and electrons in the TiO_2 layer. Notably, the HOMO levels of **TPCz-A** and **TPCz-B** are approximately 0.2 eV closer to the I^-/I_3^- redox potential than those of their indolocarbazole core counterparts. This shift may be beneficial for tuning the open-circuit voltage and could improve photovoltaic performance in DSSC devices, although additional factors also influence overall device efficiency. The LUMO energy levels meet the fundamental requirements for efficient dyes. They range from −3.18 eV to −3.39 eV, remaining above the conduction band edge of TiO_2.

This alignment is favorable for thermodynamically allowed electron injection from the excited state of the dye into the semiconductor. The calculated energy band gaps are summarized in Table 1 and illustrated in Fig. S2 in the SI.

The ΔE values for the investigated dyes fall within the range of 2.52–2.75 eV. A slight reduction in the energy gap is observed for pairs of compounds featuring identical π-linkers and acceptor groups but different donor cores (ICz and TPCz). The smallest energy band gap is calculated for **TPCz-B**, which could be attributed to the more electron-donating character of the TPCz core, leading to destabilization of the HOMO, in combination with the stronger electron-withdrawing nature of the rhodanine-3-acetic acid acceptor, which contributes to modest stabilization of the LUMO.

To obtain a more comprehensive understanding of the photovoltaic performance, the quantum-chemical calculations were further extended to the dye–TiO_2 complex systems. A $(TiO_2)_9$ cluster was implemented as a model semiconductor substrate for dye adsorption in DFT calculations. Small model clusters have previously been successfully applied to investigate the sensitization of nano-TiO_2 by structurally related dye–TiO_2 systems.[8,14,44,45] Table 2 presents the contour plots and energies of selected frontier orbitals (H−1, H, L, and L+1) for the

Table 2 The optimised structures of dye–TiO_2 complexes calculated at the B3LYP/LANL2DZ/6-31G(d,p) level in DCM, with molecular orbital contours (isovalue = 0.03) for HOMO−1, HOMO, LUMO, and LUMO+1, their corresponding energies, and energy gaps (E_{HOMO}–E_{LUMO})

Dye@TiO_2	HOMO−1 [eV]	HOMO [eV]	LUMO [eV]	LUMO+1 [eV]	ΔE [eV]
ICz-A@TiO_2	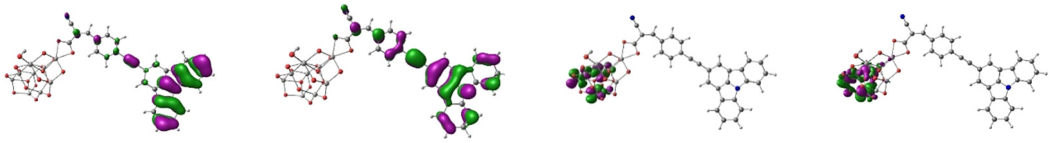				2.21
	−6.05	−5.56	−3.35	−3.22	
ICz-B@TiO_2	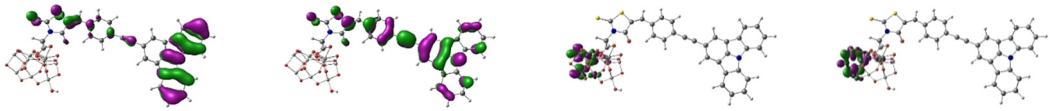				2.11
	−5.97	−5.46	−3.35	−3.22	
TPCz-A@TiO_2	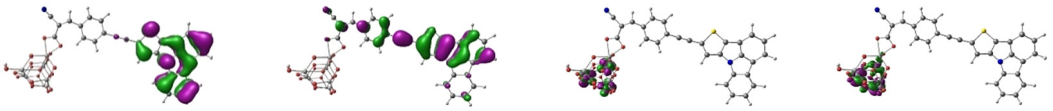				2.16
	−5.89	−5.51	−3.35	−3.23	
TPCz-B@TiO_2	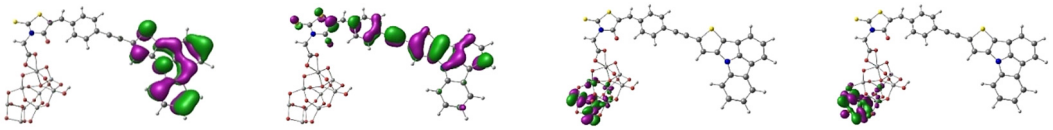				2.07
	−5.84	−5.40	−3.37	−3.23	
TPCz-C@TiO_2	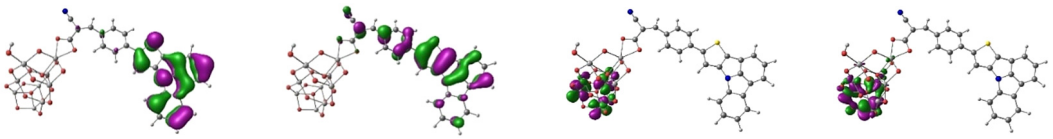				2.22
	−5.88	−5.57	−3.35	−3.22	
TPCz-D@TiO_2	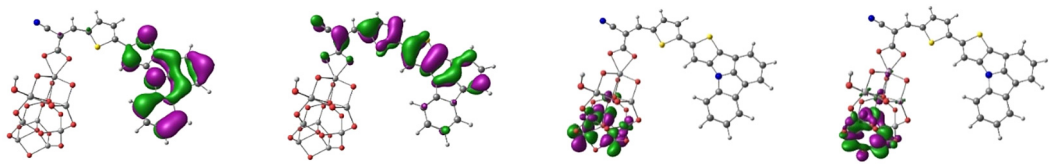				2.15
	−5.91	−5.49	−3.34	−3.21	

dyes anchored to the $(TiO_2)_9$ cluster. The occupied orbitals (H−1 and H) are predominantly localized on the donor core (ICz and TPCz), although the HOMO also shows partial delocalization onto the linker. In contrast, the unoccupied orbitals (L, L+1) are fully localized on the $(TiO_2)_9$ cluster. The energies of the HOMO increased relative to those of the isolated dyes, whereas the LUMO levels decreased slightly. As a result, the band gaps are reduced by approximately 0.5 eV compared with those of the free dyes, which is advantageous for potential photovoltaic device applications. Overall, these energy levels indicate that the investigated compounds possess sufficient driving force for use as sensitizers in DSSC devices.

It is well established that the CAM-B3LYP hybrid functional is often reported to provide improved agreement with experimental data, particularly for systems involving significant charge-transfer interactions. This functional has consistently been shown to offer a more reliable description of long-range electronic properties.[8,9,14,46–48] Accordingly, it was employed to characterize the electronic transitions in the dye-TiO_2 complexes. The simulated absorption spectra of the dye-TiO_2 complex systems are presented in Fig. S3 in the SI and are discussed in detail below. Table S2 summarizes the TD-DFT results (CAM-B3LYP/LANL2DZ; 6-31G(d,p)) for the lowest-energy absorption bands and the corresponding light-harvesting efficiency (LHE) values of the dye@TiO_2 complex systems. The LHE values were estimated using the equation: $LHE = 1–10^{-f}$, where f represents the oscillator strength of the electronic state associated with λ_{max}. Thus, LHE reflects the fraction of incident photons absorbed by the dye and can be directly related to its ability to harvest light and generate an excited state.[45,49] All investigated dyes exhibit high LHE values (>0.94), suggesting their potential for effective light harvesting in DSSC devices. However, the calculated electronic transitions are confined to a relatively narrow spectral range.

The longest-wavelength maximum transition calculated is 441 nm for the **TPCz-D**@TiO_2 complex, and the shortest absorption transition calculated is 378 nm for **ICz-A**@TiO_2.

Photophysical properties

The photophysical properties of new **ICz-A–TPCz-D** were investigated in solutions using absorption and emission spectroscopy in the UV-Vis range, data are collected in Table 3, and spectra are presented in Fig. 3. Additionally, the UV–Vis spectra of the molecules adsorbed on TiO_2, forming the photoanode in the DSSCs, were analyzed. Dye solutions in DMF ($C = 3 \times 10^{-4}$ M) were used for the preparation of the photoanodes. The UV-Vis spectra of free dyes were measured in DCM (Fig. 3a) and DMF (Fig. 3b) solutions ($C = 1 \times 10^{-5}$ M) at room temperature. The photoluminescence (PL) spectra, PL quantum yields, and lifetimes of all dyes were determined in DCM solutions ($C = 1 \times 10^{-5}$ M).

Several characteristic regions can be distinguished in the absorption spectra of dyes. Compared with DCM, the spectra recorded in DMF exhibit better-resolved and more clearly defined absorption bands. The high-energy bands observed around 280 nm originate from π–π* transitions with a strong contribution from the lone pair electrons on the central nitrogen atom.[39] In the spectral region of approximately 350–370 nm, a highly distinctive band appears, formed by π–π* transitions within the ICz and TPCz cores.[28,39] The lowest-energy absorption bands were observed around 360–450 nm. NTO analysis (Table S3 in the SI) was used to gain deeper insight into the nature of the lowest-energy electronic transition. For higher-energy excitations, which typically involve a more complex mixture of electronic configurations, the dominant molecular orbital contributions (*e.g.*, HOMO → LUMO and HOMO–1 → LUMO) are discussed to provide a qualitative description of the absorption features (Tables S5 and S7 in the SI). The absorption transition values calculated for dyes using the TD-DFT/CAM-B3LYP method, including solvent effects, show good agreement with the experimental data, with a deviation of approximately 40 nm for the lowest-energy bands.

For **ICz-A**, the main absorption band appears at approximately 350–400 nm and results from the overlap of two transitions, as indicated by TD-DFT analysis: the π–π* transition localized on the core and a transition of mixed LE/CT. In

Table 3 UV-Vis absorption and luminescence properties of **ICz-A–TPCz-D**

Dye	Absorption λ_{max} (nm) ($\varepsilon/10^4$ [$M^{-1}cm^{-1}$])			PL	
				DCM	
	DCM	DMF	TiO_2	λ_{em} (nm) [Stokes shift (cm^{-1})]	τ (ns) [weight %]	Φ (%)
ICz-A	283(0.35); 378 (0.45)	291(2.4); 348(2.6); 365 (2.4)	401	571 [7675]	1.28 [1.4330 (45.85%), 2.3728 (54.15%)]	59
ICz-B	272(3.0); 380(0.29); 422(0.4)	278(8.1); 285(4.5); 422(1.72)	437	583 [5783]	0.73 [0.3188 (16.06%), 0.7313 (80.10%), 2.4768 (3.83%)]	9
TPCz-A	278(0.67), 376(0.22), 414(0.26)	273(8.1); 368(3.4); 392(2.7); 408(2.5)	435	607 [7055]	0.68 [0.5628 (89.94%), 1.7708 (10.06%)]	17
TPCz-B	278(3.0); 342(0.29); 362(0.42); 398(0.24)	284(2.4); 311(1.9); 360(3.7); 450(2.00)	390	613 [5100]	1.27 [0.1568 (12.18%), 0.7913 (21.19%), 1.6330 (66.62%)]	16
TPCz-C	278(2.82); 376(0.26); 423(0.33)	289(0.8); 367(2.2); 394(2.0)	453	572 [5719]	1.67 [0.7613 (19.47%), 2.0756 (80.53%)]	47
TPCz-D	278(3.49); 462(0.192)	307(0.3); 376(0.7); 424(1.1); 450(0.8)	448	575 [4880]	1.06 [0.2773 (48.47%), 0.8235 (21.44%), 2.513 (30.09%)]	4

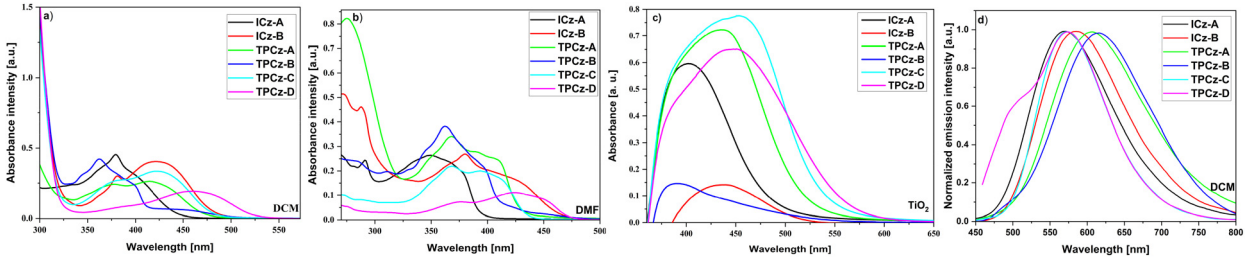

Fig. 3 The UV-Vis absorbance spectra of dyes in (a) DCM and (b) DMF ($C = 1 \times 10^{-5}$ M) and (c) upon binding to TiO_2 (glass/FTO/TiO_2@dye) and d) PL spectra in DCM of dyes ($C = 1 \times 10^{-5}$ M).

contrast, **ICz-B** exhibits significantly broader light absorption, extending up to 450 nm, which can be attributed to the presence of the rhodanine-3-acetic acid anchoring group.

Furthermore, the incorporation of the more electron-rich TPCz core leads to a pronounced broadening of the absorption spectrum. In the case of **TPCz-A**, two distinct absorption bands are observed, with the LE/CT transition red-shifted by 36 nm relative to its **ICz-A** analogue. This shift suggests enhanced push–pull interactions between the electron-rich TPCz donor and the electron-withdrawing cyanoacrylic acid anchoring group, consistent with the mixed LE/CT character of the transition. However, upon replacement of the anchoring group with rhodanine-3-acetic acid, the LE/CT band in **TPCz-B** (around 450 nm) shows reduced intensity. A similar trend is observed for **TPCz-D**, which, despite covering a broad spectral range, exhibits relatively low molar extinction coefficients.

Luo reported two structurally related dyes: 2-cyano-3-(4-(indolo[3,2,1-*jk*]carbazol-2-yl)phenyl)acrylic acid (IC-1) and 2-cyano-3-(5-(indolo[3,2,1-*jk*]carbazol-2-yl)thiophen-2-yl)acrylic acid (IC-2), and investigated their absorption and emission spectra in dichloromethane (DCM). Comparison of **ICz-A** with IC-1 indicates that the introduction of an additional acetylene bridge does not significantly alter the absorption spectral range. In contrast, for dyes containing a thiophene spacer (**TPCz-D** and IC-2), a bathochromic shift of approximately 25 nm is observed, confirming the enhanced donor strength of the TPCz core.[6]

The studied compounds adsorbed on TiO_2 exhibited absorption spectra that differed from those recorded in solution (*cf.* Fig. 3c). All dyes anchored to the TiO_2 semiconductor showed broadened absorption bands. The observed bathochromic shift in the absorption range upon binding to TiO_2 suggests the possible formation of J-aggregates (see Fig. S5 in the SI).[11,50] The broadest absorption range, extending up to 600 nm, was observed for the photoanode sensitized with the **TPCz-D** compound; however, the highest absorption intensity was recorded for TiO_2 sensitized with **TPCz-C**.

Investigation of the photoluminescence properties revealed that all the dyes exhibit orange-red emission (see Fig. 3d). The maxima of the PL band (λ_{em}) are located in the range of 571–613 nm. Comparison of analogues containing identical π-linkers and acceptor groups (**ICz-A**–**TPCz-B**) shows a pronounced bathochromic shift of approximately 33 nm in the emission maximum for the **TPCz**-Based donor systems relative to their ICz counterparts. In contrast, TPCz derivatives lacking an acetylene bridge (**TPCz-C** and **TPCz-D**) display very similar λ_{em} – around 575 nm, indicating that replacement of the spacer from phenyl to thiophene does not significantly affect the excited-state energy level. However, introduction of an additional triple bond (–C≡C–) into the D–π–A system induces a bathochromic shift in the emission maximum (**TPCz-A** – λ_{em} = 607 nm; **TPCz-C** – λ_{em} = 572 nm). A similar trend is observed for **ICz**-based systems, where **ICz-A** exhibits a red-shifted emission maximum compared to IC-2.[6]

All compounds exhibit significant Stokes shifts ranging from 4880 cm^{-1} to 7675 cm^{-1}, indicating substantial structural and electronic reorganization in the excited state. Notably, **ICz-A** and **TPCz-A**, which contain an additional acetylene bridge, display higher Stokes shift values than the other derivatives. In contrast, **TPCz-C** and **TPCz-D**, which lack an additional triple bond, exhibit comparatively smaller Stokes shifts, as expected for donor–acceptor systems. To rationalize these observations, the optimised geometries of the S_0 and S_1 states (CAM-B3LYP) were compared (Table S6 in SI). In the excited state (S_1), acetylene-linked derivatives (**ICz-A**–**TPCz-B**) exhibit a shortening of the C–C bonds between the acceptor–acetylene and donor–acetylene fragments by approximately 0.04 Å, indicating increased π-conjugation upon excitation. In contrast, derivatives without acetylene bridges (**TPCz-C** and **TPCz-D**) adopt a planar geometry in the S_1 state, whereas in the S_0 state, a twisted conformation is present, with a dihedral angle of approximately 20° between the donor units and adjacent aromatic rings. Such pronounced geometrical reorganization leads to enhanced π-conjugation and stabilization of the S_1 state relative to the S_0 minimum. In donor–acceptor systems, excited-state planarization and increased electron delocalization are often associated with an increased contribution of charge-transfer character. Therefore, the observed structural relaxation is consistent with a partial CT contribution in the emitting state, which may be associated with the large Stokes shifts.[51,52] The luminescence quantum yields of the dyes range from 4% to 59%. **ICz-A** exhibits the highest quantum yield, whereas **TPCz-D** shows the lowest.

Electrochemical properties

Following the discussion of the optical properties of the investigated ICz and TPCz derivatives, the next stage focused on their redox properties. Electrochemical investigations were

Table 4 Electron affinities (EA), ionization potentials (IP), energy band gaps (E_g), reduction and oxidation potentials (E_{red}, E_{ox} *vs.* Fc/Fc^+) and HOMO/LUMO energy levels

Dye	Method	E^1_{red} [V]	$E^{1(onset)}_{red}$ [V]	E^1_{ox} [V]	$E^{1(onset)}_{ox}$ [V]	EA [eV]	LUMO[c] [eV]	IP [eV]	HOMO[c] [eV]	E_g [eV]
ICz-A	CV	−1.54[a]	−1.28	0.95[a]	0.79	−3.82	−3.18	−5.89	−5.93	2.07
	DPV	−1.47	−1.23	0.88	0.79	−3.87		−5.89		2.02
ICz-B	CV	−1.64[b]	−1.55	0.80[a]	0.69	−3.55	−3.28	−5.79	−5.88	2.24
	DPV	−1.69	−1.62	0.80	0.69	−3.48		−5.79		2.31
TPCz-A	CV	−1.45[a]	−1.17	0.73[a]	0.62	−3.93	−3.13	−5.72	−5.77	1.79
	DPV	−1.43	−1.25	0.70	0.58	−3.85		−5.68		1.83
TPCz-B	CV	−1.65[a]	−1.44	0.75[a]	0.49	−3.66	−3.18	−5.59	−5.70	1.93
	DPV	−1.72	−1.44	0.67	0.44	−3.66		−5.54		1.88
TPCz-C	CV	−1.63[a]	−1.26	0.83[a]	0.69	−3.84	−3.22	−5.79	−5.95	1.95
	DPV	−1.58	−1.27	0.86	0.74	−3.84		−5.84		2.00
TPCz-D	CV	−1.54[a]	−1.28	0.79[a]	0.56	−3.82	−3.39	−5.66	−5.94	1.84
	DPV	−1.57	−1.21	0.76	0.65	−3.89		−5.75		1.86

$IP = (-5.1 - E^{1(onset)}_{ox})\cdot e^-$, $EA = (-5.1 - E^{1(onset)}_{red})\cdot e^-$, $E_g = E^{1(onset)}_{ox} - E^{1(onset)}_{red}$. Solvent: DCM with a concentration of 1×10^{-3} M; electrolyte: Bu_4NPF_6 with a concentration of 1×10^{-1} M; Pt as the working electrode. [a] Irreversible process. [b] Quasi-reversible process. E^1_{ox} – the first oxidation process, E^1_{red} – the first reduction process, $E^{1(onset)}_{red}$ – the onset potential of the first reduction process, $E^{1(onset)}_{ox}$ – the onset potential of the first oxidation process. [c] LUMO and HOMO estimated by theoretical calculations (B3LYP/6-311G(d,p) in DCM). The redox data reported used IUPAC convention.

performed using cyclic voltammetry (CV) and differential pulse voltammetry (DPV) in DCM solution containing tetrabutylammonium hexafluorophosphate (Bu_4NPF_6) as the supporting electrolyte.

A platinum electrode was employed as the working electrode, and all potentials were referenced to the ferrocene/ferrocenium (Fc/Fc^+) redox couple. The onset potentials of the first oxidation and reduction peaks (*vs.* Fc/Fc^+) were employed to estimate the IP (ionization potentials) and EA (electron affinities), respectively. The resulting EA and IP values with energy band gaps, oxidation and reduction potentials and HOMO/LUMO energy levels are collected in Table 4 and Table S9 in the SI, while selected voltammograms are presented in Fig. 4 and Fig. S4 in the SI.

The first irreversible cathodic peak corresponding to the reduction process was recorded in the potential range of −1.43 to −1.72 V *vs.* Fc/Fc^+ (*cf.* Fig. 4a). An exception was observed for **ICz-B**, which exhibited a quasi-reversible reduction process (ΔE_p = 90 mV). The reduction occurred most readily for **TPCz-A** (E^1_{red} = −1.45 V), **ICz-A** (E^1_{red} = −1.54 V), and **TPCz-D** (E^1_{red}= −1.54 V), which contain the 2-cyano-3-phenylacrylic acid substituent (**ICz-A**, **TPCz-A**) or 2-cyano-3-(thiophen-2-yl)acrylic acid (**TPCz-D**). For **ICz-A** and **TPCz-A**, subsequent reduction processes were observed at $E^2_{red} \approx -2.11$ V and $E^3_{red} \approx -2.50$ V, respectively (Table S9). In contrast, no further reduction processes were observed for **TPCz-D**. However, for **TPCz-C**, the second and third reduction processes were recorded at E^2_{red} = −2.13 V and E^3_{red} = −2.31 V, respectively. Moreover, **TPCz-C**, which incorporates a thiophene unit in the TPCz core and lacks an acetylene linker, exhibited a shift of the first reduction peak toward more negative potentials (E^1_{red} = −1.63 V) compared to **ICz-A** and **TPCz-A** (*cf.* Fig. 4c).

The reduction process is associated with the presence of the cyanoacrylic acid acceptor group (–CH═–C(CN)COOH). The first reduction step is most likely related to a one-electron electrochemical reduction of the strongly electron-withdrawing nitrile group, leading to the formation of a radical anion or alternatively the reduction of the conjugated C═C–C≡N moiety.

The latter process typically occurs at more negative potentials and is irreversible, compared to other functional groups such as carboxylic acids.[53] The subsequent reduction peak is likely due to further reduction of previously generated radical species. The first reduction peaks for **ICz-B** and **TPCz-B** bearing the rhodanine-3-acetic acid substituent (due to the presence of dihydrothiophene-2(3*H*)-thione) were the most negatively shifted (E^1_{red} = −1.64 to −1.72 V) (*cf.* Fig. 4b).

The similarity of the E^1_{red} values for these compounds indicates a weak influence of the core on the reduction process although only the **TPCz-B** compound exhibited a second reduction peak. The irreversible oxidation process is associated with the TPCz and ICz core with the formation of an unstable radical cation.[39] Oxidation of TPCz occurred more willingly. This behavior can be attributed to the reduction occurring predominantly on the rhodanine moiety, facilitated by the presence of sulfur atoms. However, for **TPCz-C** the first oxidation peak was recorded at E^1_{ox} = 0.83 V, with no further oxidation processes observed (*cf.* Table S9).

The LUMO energy levels are strongly influenced by the nature of the acceptor substituent, as was mentioned in the DFT calculations. Compounds bearing the rhodanine-3-acetic acid unit (**ICz-B** and **TPCz-B**) exhibit the most negatively shifted reduction onset potentials, resulting in relatively raised LUMO levels (EA ≈ −3.55 eV to −3.66 eV, respectively). In contrast, compounds lacking the (4-oxo-2-thioxo-1,3-thiazolidin-3-yl)-acetic acid group show lower LUMO levels, reaching values of up to −3.93 eV for **TPCz-A**, indicating enhanced electron affinity.

The HOMO energy levels are mainly dependent on the donor core and vary within a relatively narrow range (IP ≈ −5.54 to −5.89 eV). Derivatives based on the TPCz core generally display slightly higher-lying HOMO levels compared to their ICz counterparts, which is consistent with the lower oxidation onset potentials observed for the TPCz series. This is due to the

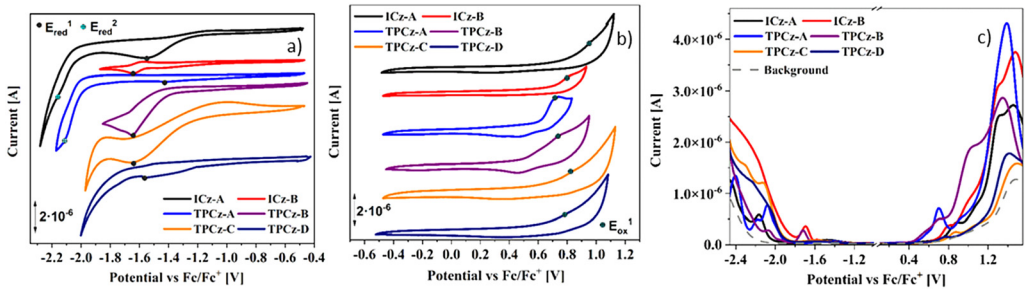

Fig. 4 Voltammograms of (a) reduction and (b) oxidation processes obtained by cyclic voltammetry (CV) and (c) reduction and oxidation processes obtained by differential pulse voltammetry (DPV) (Pt, CH_2Cl_2, 1×10^{-1} M Bu_4NPF_6, scan rate of 100 mV s^{-1}).

presence of a thiophene ring in the core, which increases electron donation ability and destabilises the HOMO level. The electrochemical energy gaps ranged from 1.79 to 2.31 eV. The narrowest energy gaps ($\approx$1.8 eV) were obtained for **TPCz-A** and **TPCz-D**, whereas **ICz-B** exhibits the largest E_g value (up to 2.31 eV), primarily due to rhodanine-induced LUMO.

It can be concluded that, considering the frontier molecular orbital energy levels of the studied compounds, they appear to be suitable for application in DSSCs. Their LUMO energy levels are higher than the conduction band edge of TiO_2 (4.0 eV), while their HOMO energy levels are lower than the I^-/I_3^- redox potential (4.8 eV).

Photovoltaic performance

The synthesized compounds were employed as light-harvesting dyes in dye-sensitized solar cells. Based on the UV–Vis spectra of the fabricated photoanodes (*cf.* Fig. 3c), two of them, sensitized with **ICz-B** and **TPCz-B**, exhibited narrower absorption ranges along with noticeably lower absorbance values, which may result in reduced photovoltaic performance of the DSSC devices.

In turn, compounds lacking the acetylene bridge (**TPCz-C** and **TPCz-D**) exhibited the broadest absorption range, with **TPCz-C** showing relatively higher absorbance. Therefore, it can be expected that devices sensitized with these dyes may demonstrate comparatively higher performance, consistent with their more favorable optical characteristics.

However, at the initial stage of the study, a standard solar cell architecture (glass/FTO/m-TiO_2@dye/EL-HSE/Pt/FTO/glass) incorporating solely the investigated dye molecules as a photosensitizer was fabricated to identify the most promising pyrrolocarbazole derivative based on the measured photovoltaic parameters. The PV performance was evaluated using four key parameters: the open-circuit voltage, the short-circuit current density, the fill factor (FF), and the power conversion efficiency (PCE), as determined from the recorded current–voltage (*J–V*) characteristic. Table 5 summarizes the photovoltaic parameters of solar cells based on the investigated dyes, as extracted from the recorded *J–V* characteristics (Fig. 5) measured under standard illumination conditions (100 mW cm^{-2}). The average photovoltaic parameters were determined from

Table 5 Photovoltaic parameters of solar cells based on indolo[3,2,1-*jk*]carbazole and thienopyrrolo[3,2,1-*jk*]carbazole derivatives under standard illumination conditions

Photoanode structure	V_{oc} [mV]	J_{sc} [mA cm^{-2}]	FF	PCE [%]
Glass/m-TiO_2@N719	740	15.43	0.51	5.74
Glass/m-TiO_2@**ICz-A**	554	0.54	0.55	0.16
Glass/m-TiO_2@**ICz-B**	306	0.07	0.46	0.01
Glass/m-TiO_2@**TPCz-A**	599	1.59	0.58	0.54
Glass/m-TiO_2@**TPCz-B**	192	0.02	0.37	0.00
Glass/m-TiO_2@**TPCz-C**	602	4.05	0.54	1.31
Glass/m-TiO_2@**TPCz-D**	566	2.46	0.55	0.77

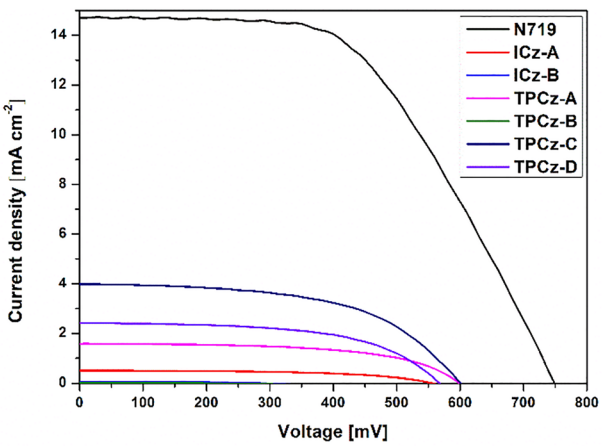

Fig. 5 The current density–voltage curves of solar cells based on investigated dyes obtained under standard illumination conditions (100 mW cm^{-2}).

measurements of three identical solar cells fabricated under identical conditions.

An analysis of the data presented in Table 5 indicates that, in agreement with the expectations based on the optical properties of the photoanodes, the application of **TPCz-C** proved to be the most advantageous. Among the six investigated carbazole derivatives, devices sensitized with **TPCz-C** exhibited the highest average PCE of 1.31%.

Moreover, the photocurrent densities correlate well with the absorption characteristics of the corresponding photoanodes.

As anticipated from its broad absorption range and high absorbance, the photoanode incorporating **TPCz-C** yielded the highest average J_{sc} of 4.05 mA cm^{-2}. A lower J_{sc} value was observed for devices based on **TPCz-D** (2.46 mA cm^{-2}), whereas the lowest values were recorded for DSSCs sensitized with **ICz-B** and **TPCz-B**, amounting to 0.07 and 0.02 mA cm^{-2}, respectively. For DSSCs sensitized with **ICz-B** and **TPCz-B**, the extremely low J_{sc} values translated into PCE values close to 0%. Such a trend could be anticipated from the UV–Vis absorption characteristics of the dyes immobilized on TiO_2. For comparison, reference solar cells based on the commercial dye N719 were prepared, yielding an average PCE of 5.74%.

For selected DSSCs, the photovoltaic parameters were preliminarily evaluated at reduced light intensities in the range of 10–80 mW cm^{-2}. Only fully operational devices were included in the analysis; solar cells sensitized with **ICz-B** and **TPCz-B** dyes were excluded. For the remaining series, one representative device for each carbazole derivative was selected and subjected to detailed characterization. The photovoltaic parameters determined from the current–voltage curves (Fig. 6) recorded at reduced illumination intensities are summarized in Table S10 in the SI.

The evaluation of PV parameters at reduced illumination intensities was performed to assess the potential applicability of the devices under indoor photovoltaic conditions. For DSSCs sensitized with **TPCz-C** or **TPCz-D**, which showed higher efficiencies under standard conditions, an increase in performance was observed as the light intensity was reduced. In contrast, DSSCs incorporating **ICz-A** and **TPCz-A** exhibited decreasing PCE with decreasing light intensity. A notably larger decrease in V_{oc} was observed for these devices compared to those based on **TPCz-C** and **TPCz-D**. This behavior may be attributed, at least in part, to a pronounced increase in series resistance. At 100 mW cm^{-2}, the series resistances of **ICz-A** and **TPCz-A** devices were 188 and 73 Ω, respectively, rising to 3422 and 525 Ω at 10 mW cm^{-2}.

By comparison, the series resistances of **TPCz-C** and **TPCz-D** devices changed less dramatically, from 53 and 66 Ω at 100 mW cm^{-2} to 169 and 218 Ω at 10 mW cm^{-2}, respectively. A reduction in V_{oc} was consistently observed across all examined devices. As an example, the **TPCz-C**-based device exhibited a decrease in V_{oc} from 601 to 534 mV. Moreover, the variation of V_{oc} with light intensity can be primarily attributed to two key processes occurring within the solar cell, namely, charge generation and charge carrier lifetime.

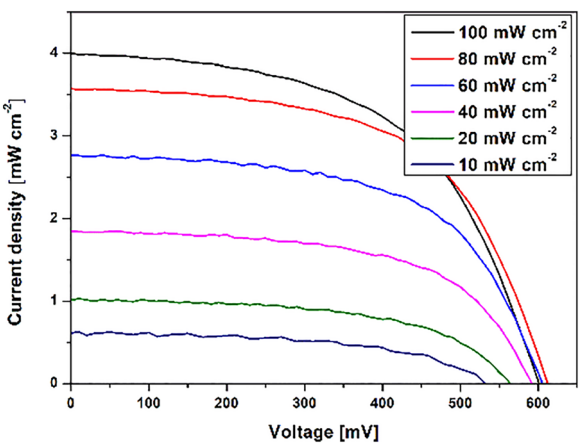

Fig. 6 Current density–voltage curves of solar cells containing **TPCz-C** under reduced illumination.

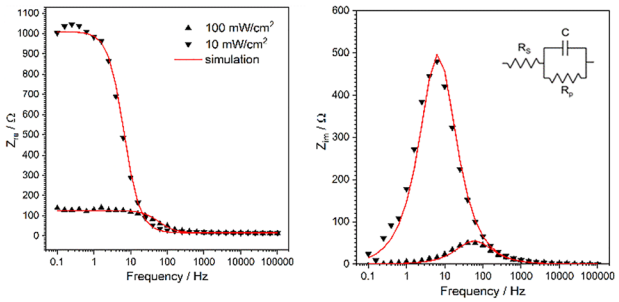

Fig. 7 Impedance spectra of the **TPCz-A** based device: real (on the left) and imaginary (on the right) part as functions of frequency for high and low light intensities (upward and downward triangle data points), under open-circuit conditions. The red line illustrates fitting to the equivalent circuit model shown in the inset.

The increase in V_{oc} at higher illumination levels arises because the rate of charge generation increases more rapidly with light intensity than the corresponding decrease in charge lifetime. In contrast, under reduced illumination, the influence of the charge lifetime becomes more dominant relative to the generation rate, leading to a decline in V_{oc}.[54]

To gain more insight into the illumination effect on charge-transfer, the impedance spectra were recorded and analysed under open-circuit conditions and at varying light intensities. Fig. 7 shows a typical comparison of the impedance spectra at high and low light intensities.

The analysis of impedance spectra gives the values of double-layer capacitance (C), charge transfer resistance (R_p) and the series resistance (R_s).

It is important to know that the parameters describe the system response to the alternating voltage signal and are different from the series resistance calculated from the current–voltage curve mentioned above. All the devices reveal a similar double-layer capacitance of about 24 μF and an R_s of about 17 Ω at both high and low light intensities. This fact confirms that the photoanodes of all the devices have a similar surface area, and the electrode connections were stable. The R_p resistance is the only parameter that reveals a strong dependence on light intensity. As compared above, the charge transfer resistance of **ICz-A** and **TPCz-A** based devices are 86.7 and 110 Ω, respectively, at 100 mW cm^{-2} and rise about ten times to 851 and 994 Ω, respectively, at 10 mW cm^{-2}.

Generally, J_{sc} scales proportionally with light intensity and typically follows a near-linear relationship.[55] For the **TPCz-C**-based device, J_{sc} likewise decreased, from 4.05 to 0.62 mA cm^{-2}, consistent with the anticipated behaviour under reduced illumination. This behaviour reflects the direct proportionality between the incident photon flux and the number of

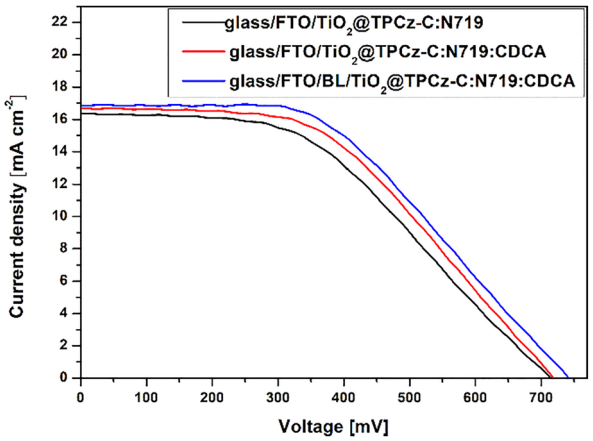

Fig. 8 Current density–voltage curves of modified solar cells containing **TPCz-C**.

photogenerated charge carriers, resulting in an almost linear increase in current under standard operating conditions. Since the device incorporating **TPCz-C** exhibited the highest efficiency (1.77% at 10 mW cm^{-2}, see Table S10 in the SI), this dye was chosen for subsequent investigations and structural modifications to enhance the photovoltaic performance.

Since the highest photovoltaic performance was obtained for DSSCs sensitized with **TPCz-C**, additional strategies were implemented to further enhance device efficiency. To explain the effect of each modification, the approaches were introduced sequentially. Initially, co-sensitization with a **TPCz-C**:N719 dye mixture was applied, yielding a device with the architecture glass/FTO/m-TiO_2@**TPCz-C**:N719/EL-HSE/Pt/FTO/glass.

Subsequently, chenodeoxycholic acid (CDCA) was introduced as a co-adsorbent to suppress dye aggregation on the TiO_2 surface, resulting in the configuration glass/FTO/m-TiO_2@**TPCz-C**:N719:CDCA/EL-HSE/Pt/FTO/glass. In the final step, a compact TiO_2 blocking layer (BL) prepared from a $TiCl_4$ precursor was incorporated, affording the device structure glass/FTO/BL-TiO_2/m-TiO_2@**TPCz-C**:N719:CDCA/EL-HSE/Pt/FTO/glass. The current–density curves of tested DSSCs are shown in Fig. 8, and the photovoltaic parameters are summarized in Table 6.

According to the data presented in Table 6, an enhancement in device performance was observed compared to the initial device sensitized solely with **TPCz-C** (1.33%). The solar cell featuring the photoanode architecture glass/m-TiO_2@**TPCz-C**:N719 exhibited an average PCE of 5.17%, which was slightly lower than that of the reference device based exclusively on N719 (5.74%). Notably, however, this approach enabled a substantial reduction in the amount of commercial dye employed, which may have important implications for reducing the overall fabrication costs of the solar cells.

The incorporation of CDCA as a co-adsorbent, aimed at suppressing dye aggregation on the TiO_2 surface, led to a further increase in PCE to nearly 5.60%. This improvement was primarily associated with an increase in J_{sc}, likely resulting from the suppression of unfavourable charge recombination processes and, consequently, more efficient electron generation.

The introduction of a thin TiO_2 blocking layer, further suppressing charge recombination, resulted in an additional improvement in the photovoltaic parameters. In particular, the short-circuit current density increased by 0.55 mA cm^{-2}, while the FF increased from 0.46 to 0.50. The enhancement of these parameters led to a PCE of 6.20%.

DSSCs with the modified configuration were further investigated with respect to their applicability under illumination ten times lower than the standard value. The light intensity was decreased stepwise from 100 to 10 mW cm^{-2} (10 mW cm^{-2} increments) to systematically monitor changes in the *J*–*V* curves (Fig. S6 in the SI) and the resulting PV parameters. The collected values of V_{oc}, J_{sc}, FF, and PCE are summarized in Table 7.

Table 6 Photovoltaic parameters of selected solar cells based on indolo[3,2,1-*jk*]carbazole and thienopyrrolo[3,2,1-*jk*]carbazole derivatives under standard illumination conditions (10 mW cm^{-2})

Photoanode structure	V_{oc} [mV]	J_{sc} [mA cm^{-2}]	FF	PCE [%]
Glass/m-TiO_2@**TPCz-C**:N719	722	15.83	0.46	5.17
Glass/m-TiO_2@**TPCz-C**:N719:CDCA	726	16.85	0.46	5.59
Glass/BL/m-TiO_2@ **TPCz-C**:N719:CDCA	732	17.40	0.50	6.20

Table 7 Photovoltaic parameters of modified solar cells based on **TPCz-C** under reduced illumination conditions

Photoanode structure	Light intensity [mW cm^{-2}]	V_{oc} [mV]	J_{sc} [mA cm^{-2}]	FF	PCE [%]
Glass/m-TiO_2@**TPCz-C**:N719	100	722	15.83	0.46	5.17
	90	711	14.76	0.49	5.69
	80	707	13.04	0.51	5.98
	70	703	11.47	0.54	6.27
	60	698	9.97	0.57	6.56
	50	693	8.14	0.59	6.88
	40	687	6.84	0.62	7.30
	30	679	5.38	0.63	7.73
	20	667	3.79	0.67	8.47
	10	648	2.39	0.68	10.42
Glass/m-TiO_2@**TPCz-C**:N719:CDCA	100	726	16.85	0.46	5.59
	90	717	14.91	0.50	5.93
	80	713	13.34	0.53	6.30
	70	711	11.70	0.56	6.58
	60	706	10.01	0.57	6.72
	50	700	8.53	0.60	7.10
	40	695	6.92	0.64	7.66
	30	683	5.16	0.67	7.92
	20	672	3.76	0.69	8.65
	10	658	2.26	0.71	10.76
Glass/BL/m-TiO_2@**TPCz-C**:N719:CDCA	100	732	17.40	0.50	6.20
	90	739	15.27	0.51	6.34
	80	735	13.58	0.53	6.65
	70	730	12.00	0.55	6.93
	60	726	10.32	0.57	7.32
	50	722	8.55	0.62	7.70
	40	717	7.11	0.64	8.11
	30	710	5.48	0.67	8.71
	20	699	3.90	0.72	9.78
	10	686	2.37	0.78	12.30

Based on the data presented in Table 7, the PCE was found to increase with decreasing light intensity, as anticipated. The observed trend was consistent with that noted for the standard device architecture and for cells based on **TPCz-C** and **TPCz-D** (Table S10 in the SI). For the modified devices incorporating **TPCz-C**, a decrease in V_{oc} of 46–74 mV was observed when comparing measurements at 100 and 10 mW cm^{-2}. As expected, due to the lower photon flux reaching the active layer under reduced illumination, the J_{sc} decreased in all cases by approximately 86%. Notably, however, the FF increased substantially, by as much as 55% (48% for **TPCz-C**:N719). In contrast to the trends observed for V_{oc} and J_{sc}, the FF exhibited an opposite dependence on light intensity, increasing as the illumination level decreased. This behaviour can be attributed to the reduced photocurrent at lower light intensities, which diminishes voltage losses associated with series resistance and suppresses electron recombination, thereby enhancing the fill factor.[56] In line with the FF trend, the power conversion efficiency increased with decreasing light intensity. Upon reducing the light intensity to 10 mW cm^{-2}, the device incorporating the **TPCz-C**:N719 dye mixture achieved a PCE of 10.42%. The introduction of CDCA further improved the efficiency to 10.76%. A subsequent modification involving the incorporation of a blocking layer resulted in an additional enhancement of nearly 15%, yielding a final PCE of 12.30%. Overall, the sequential implementation of co-sensitization, co-adsorbent incorporation, and blocking layer deposition proved to be an effective strategy for enhancing device performance under low-light conditions, highlighting the potential of the optimised architecture for indoor photovoltaic applications.

Conclusions

Six novel D–π–A systems were successfully synthesized and comprehensively investigated. Tripod rigid-skeleton cores (ICz and TPCz) were employed as electron-donating units, while strong electron acceptors—cyanoacrylic acid and rhodanine-3-acetic acid—were introduced through phenyl or thiophene π-linkers, with or without an additional acetylene spacer. Despite their structurally simple molecular architectures, the dyes exhibited broad light absorption, reaching up to 520 nm in solution and extending to approximately 600 nm upon adsorption onto TiO_2. All compounds displayed orange-red photoluminescence accompanied by pronounced Stokes shifts.

Quantum-chemical calculations revealed that the HOMOs are predominantly localized on the donor cores (ICz and TPCz), whereas the LUMOs are mainly distributed over the acceptor moieties, confirming the expected intramolecular charge-transfer character. Incorporation of sulfur into the conjugated core (TPCz) resulted in modulation of the frontier orbital energy levels, including a lowering of the HOMO energy.

Although numerous literature reports, largely based on DFT calculations, have suggested that **ICz**-based systems are promising candidates for DSSC photosensitizers, the **ICz-A** and **ICz-B** dyes investigated herein did not demonstrate satisfactory photovoltaic performance under the applied experimental conditions. DSSC devices with a standard architecture (glass/FTO/m-TiO_2@dye/EL-HSE/Pt/FTO/glass), employing the synthesized dyes as sole photosensitizers, were fabricated. However, these devices exhibited relatively low power conversion efficiencies (PCEs) under standard illumination (100 mW cm^{-2}). The highest PCE achieved in this series was 1.31% for devices sensitized with **TPCz-C**.

To improve device performance, the cell architecture was systematically optimised. The photosensitization process was enhanced through co-sensitization with N719 and the use of CDCA as a co-adsorbent, combined with the introduction of a blocking layer. The resulting architecture (glass/FTO/BL-TiO_2/m-TiO_2@**TPCz-C**:N719:CDCA/EL-HSE/Pt/FTO/glass) exhibited a significantly improved PCE of 6.20% under standard illumination.

To evaluate the potential of the optimised architecture for low-intensity photovoltaic application, the *J*–*V* curves and PV parameters were monitored under reduced illumination from 100 to 10 mW cm^{-2}. Upon decreasing the light intensity to 10 mW cm^{-2}, the highest power conversion efficiency achieved was was 12.30% for solar cells containing **TPCz-C**:N719:CDCA and the introduced blocking layer. These results demonstrate that **TPCz**-Based D–π–A systems, particularly when implemented within an optimised device architecture, are promising candidates for low-intensity photovoltaic applications, with potential relevance to emerging indoor energy-harvesting technologies.

Conflicts of interest

There are no conflicts to declare.

Data availability

The authors confirm that the data supporting the findings of this study have been included as part of the supplementary information (SI). Supplementary information: experimental details, measurements, calculations, synthesis and characterization. See DOI: https://doi.org/10.1039/d6tc00689b. The data that support the findings of this study are openly available in [https://repod.icm.edu.pl] at https://doi.org/10.18150/HHDXIX.

Acknowledgements

This research was funded by the National Science Centre of Poland Grant: no. 2020/39/D/ST5/00104. Calculations were carried out using resources provided by the Wroclaw Centre for Networking and Supercomputing (http://wcss.pl), grant no. 18. Research on DSSCs was carried out with financial support from the National Science Centre under the Miniatura programme (project number: DEC-2024/08/X/ST5/01301). As part of the Miniatura programme, essential reagents were purchased to enable the preparation of selected solar cell components. For the purpose of Open Access, the authors have applied a CC-BY

References

1 H. Zhou, M. Aftabuzzaman, S. H. Kang and H. K. Kim, *ACS Energy Lett.*, 2025, **10**, 881.
2 S. Rahman, A. Haleem, M. K. Hussain, M. Siddiq, S. Qamar, S. Hameedd and M. Waris, *RSC Adv.*, 2023, **13**, 19508.
3 Q. C. A. Al-Furaiji, H. A. Hasan, W. N. A. Al-Mehana, A. M. Alraih, M. A. Mohammed, G. Abdulkareem-Alsultan and M. F. Nassar, *J. Mol. Struct.*, 2026, **1349**, 143833.
4 K. S. Keremane, I. M. Abdellah, M. R. Eletmany, P. Naik, P. Aneesg and A. V. Adhikari, *J. Mater. Chem. C*, 2025, **13**, 9258.
5 Y. Jiao, S. Liu, Z. Shen, L. Mao, Y. Ding, D. Ren, F. T. Eickemeyer, L. Pfeifer, D. Cao, W. Xu, J. Song, B. Mi, Z. Gao, S. M. Zakeeruddin, W. Huang and M. Grätzel, *J. Mater. Chem. A*, 2021, **9**, 26311.
6 C. Luo, W. Bi, S. Deng, J. Zhang, S. Chen, B. Li, Q. Liu, H. Peng and J. Chu, *J. Phys. Chem. C*, 2014, **118**, 14211.
7 J. Sivanadanam, P. Ganesan, P. Gao, M. K. Nazeeruddin, A. Emeline, D. Bahnemann and R. Rajalingam, *RSC Adv.*, 2016, **6**, 37347.
8 D. Zych and A. Slodek, *J. Mol. Struct.*, 2020, **1207**, 127771.
9 Q. C. A. Al-Furaiji, H. A. Hasan, W. N. A. Al-Mehana, A. M. Alraih, M. A. Mohammed, G. Abdulkareem-Alsultan and M. F. Nassar, *J. Mol. Struct.*, 2026, **1353**, 144747.
10 C. L. Boldrini, P. Biagini, V. Capriati, A. F. Quivelli, A. Abbotto, F. M. Perna and N. Manfredi, *Sustainable Energy Fuels*, 2024, **8**, 504.
11 B. Hemavathi, V. Jayadev, S. C. Pradhan, G. Gokul, K. Jagadish, G. K. Chandrashekara, P. C. Ramamurthy, R. K. Pai, K. N. N. Unni, T. N. Ahipa, S. Soman and R. G. Balakrishna, *Sol. Energy*, 2018, **174**, 1085.
12 I. Abubakari, *Comput. Theor. Chem.*, 2025, **1248**, 115165.
13 R. Munir, A. F. Zahoor, M. N. Anjum, U. Nazeer, A. U. Haq, A. Mansha, A. R. Chaudhry and A. Irfan, *Top. Curr. Chem.*, 2025, **383**, 5.
14 P. Gnida, S. Zimosz, A. Glinka, M. Ziółek, D. Zych, S. Kotowicz, M. F. Amin, P. Chulkin, G. Kulesza-Matlak, A. Slodek and E. Schab-Balcerzak, *Ind. Eng. Chem. Res.*, 2024, **63**, 7133.
15 S. Zimosz, A. Slodek, P. Gnida, A. Glinka, M. Ziółek, D. Zych, A. K. Pająk, M. Vasylieva and E. Schab-Balcerzak, *J. Phys. Chem. C*, 2022, **126**, 8986.
16 P. Gnida, A. Slodek, P. Chulkin, M. Vasylieva, A. K. Pająk, A. Seweryn, M. Godlewski, B. S. Witkowski, G. Szafraniec-Gorol and E. Schab-Balcerzak, *Dyes Pigm.*, 2022, **200**, 110166.
17 A. Slodek, D. Zych, G. Szafraniec-Gorol, P. Gnida, M. Vasylieva and E. Schab-Balcerzak, *Materials*, 2020, **13**, 2292.
18 A. Slodek, D. Zych, S. Golba, S. Zimosz, P. Gnida and E. Schab-Balcerzak, *J. Mater. Chem. C*, 2019, **7**, 5830.
19 K. E. Roys, S. L. Manju, M. Siddiq and A. Sambandam, *RSC Adv.*, 2024, **14**, 29229.
20 K. E. Roys and S. L. Manju, *J. Mol. Struct.*, 2024, **1304**, 137662.
21 W. Cao, M. Fang, Z. Chai, H. Xu, T. Duan, Z. Li, X. Chen, J. Qin and H. Han, *RSC Adv.*, 2015, **5**, 32967.
22 D. Zhang, Q. Wang, J. Zhou, W. Yuan, C. Cheng, J. Wei, D. Zhang and L. Duan, *Angew. Chem., Int. Ed.*, 2025, **64**, e202517349.
23 M. R. S. A. Janjua, M. U. Khan, M. Khalid, N. Ullah, R. Kalgaonkar, K. Alnoaimi, N. Baqader and S. Jamil, *J. Cluster Sci.*, 2021, **32**, 243.
24 H. Dua, D. Paul and U. Sarkar, *Phys. Chem. Chem. Phys.*, 2025, **27**, 2720.
25 A. Ammasi and A. P. Munusamy, *Struct. Chem.*, 2018, **29**, 967.
26 S. Bibi, S. Ashraf, S. Ismaeel, S. UrRehman, S. Jamil, M. A. Iqbal, S. R. Khan, S. G. Khan and H.-X. Zhang, *Optik*, 2025, **339**, 172550.
27 K. A. Samawi, E. A.-A. Salman, B. A.-A. Alshekhly, M. F. Nassar, M. Y. Borzehandani, G. Abdulkareem-Alsultan, M. A. M. Latif and E. Abdulmalek, *Comp. Theor. Chem.*, 2022, **1212**, 113725.
28 G. Szafraniec-Gorol, D. Zych, S. Kotowicz, S. Zimosz, M. Siwy, E. Schab-Balcerzak, M. Szalkowski, S. Mackowski and A. Slodek, *Chem. Phys. Chem.*, 2025, **26**, e202500072.
29 G. Szafraniec-Gorol, A. Slodek, D. Zych, M. Vasylieva, M. Siwy, K. Sulowska, S. Mackowski, I. Taydakov, D. Goriachiy and E. Schab-Balcerzak, *J. Mater. Chem. C*, 2021, **23**, 7351.
30 V. V. Patil, W. P. Hong and J. Y. Lee, *Adv. Energy Mater.*, 2025, **15**, 2400258.
31 X.-F. Luo, H.-X. Ni, L. Shen, L. Wang, X. Xiao and Y.-X. Zheng, *Chem. Commun.*, 2023, **59**, 2489.
32 Y. Wang and G. Zhang, *Eur. J. Org. Chem.*, 2022, e202200494.
33 Q.-M. Liu, L. Yuan, X.-J. Liao, X.-S. Zhong, H.-X. Ni, Y. Wang, Y. Zhao and Y.-X. Zheng, *Mater. Chem. Front.*, 2023, **7**, 4944.
34 Z.-Z. Qu, X.-F. Luo, M.-X. Mao, C.-F. Yip, Y.-X. Zheng and J.-L. Zuo, *Adv. Energy Sustainabilty Res.*, 2022, **3**, 2200057.
35 F. Zhong, B. Zhang, Y. Huang, B. Li, X. He, Z. Wang and B. Z. Tang, *Adv. Opt. Mater.*, 2025, **13**, 2403538.
36 I. Hajji, M. Petković, A. M. Alraih, A. K. Hajri, I. Zghab, Z. H. Alnakhli and F. Aloui, *J. Mol. Struct.*, 2025, **1321**, 140104.
37 D. Tavgeniene, R. Beresneviciute, D. Blazevicius, G. Krucaite, G. Jacunskaite, S. S. Swayamprabha, J.-H. Jou and S. Grigalevicius, *Coatings*, 2022, **12**, 932.
38 R. Bisht, V. Sudhakar, M. F. M. Kavungathodi, N. Karjule and J. Nithyanandhan, *ACS Appl. Mater. Interfaces*, 2018, **10**, 26335.
39 D. Bader, J. Fröhlich and P. Kautny, *J. Org. Chem.*, 2020, **85**, 3865.
40 Y. S. Tingare, N. S. Vinh, H.-H. Chou, Y.-C. Liu, Y.-S. Long, T.-C. Wu, T.-C. Wei and C.-Y. Yeh, *Adv. Energy Mater.*, 2017, **7**, 1700032.
41 S. Venkatesan, W.-H. Lin, T.-H. Hsu, H. Teng and Y.-L. Lee, *ACS Sustainable Chem. Eng.*, 2022, **10**, 2473.

42 M. J. Frisch, G. W. Trucks, H. B. Schlegel, G. E. Scuseria, M. A. Robb, J. R. Cheeseman, G. Scalmani, V. Barone, G. A. Petersson, H. Nakatsuji, X. Li, M. Caricato, A. V. Marenich, J. Bloino, B. G. Janesko, R. Gomperts, B. Mennucci, H. P. Hratchian, J. V. Ortiz, A. F. Izmaylov, J. L. Sonnenberg, D. Williams-Young, F. Ding, F. Lipparini, F. Egidi, J. Goings, B. Peng, A. Petrone, T. Henderson, D. Ranasinghe, V. G. Zakrzewski, J. Gao, N. Rega, G. Zheng, W. Liang, M. Hada, M. Ehara, K. Toyota, R. Fukuda, J. Hasegawa, M. Ishida, T. Nakajima, Y. Honda, O. Kitao, H. Nakai, T. Vreven, K. Throssell, J. A. Montgomery, Jr., J. E. Peralta, F. Ogliaro, M. J. Bearpark, J. J. Heyd, E. N. Brothers, K. N. Kudin, V. N. Staroverov, T. A. Keith, R. Kobayashi, J. Normand, K. Raghavachari, A. P. Rendell, J. C. Burant, S. S. Iyengar, J. Tomasi, M. Cossi, J. M. Millam, M. Klene, C. Adamo, R. Cammi, J. W. Ochterski, R. L. Martin, K. Morokuma, O. Farkas, J. B. Foresman, and D. J. Fox, *Gaussian 16 (Revision C.01)*, Gaussian, Inc., Wallingford CT, 2016.
43 G. Scalmani and M. J. Frisch, *J. Chem. Phys.*, 2010, **132**, 114110.
44 R. Sanchez-De-Armas, M. A. San-Miguel, J. Oviedo, A. Márquez and J. F. Sanz, *Phys. Chem. Chem. Phys.*, 2011, **13**, 1506.
45 S. A. Alrub, A. I. Ali, R. K. Hussein, S. K. Alghamdi and S. A. Eladly, *Int. J. Mol. Sci.*, 2024, **25**, 5586.
46 T. Yanai, D. P. Tew and N. C. Handy, *Chem. Phys. Lett.*, 2004, **393**, 51.
47 J.-D. Chai and M. Head-Gordon, *Phys. Chem. Chem. Phys.*, 2008, **10**, 6615.
48 F. A. AL-Temimei, *Opt. Quantum Electron.*, 2022, **54**, 600.
49 A. Barak, N. Dhiman, F. Sturm, F. Rauch, Y. A. Lakshmanna, K. S. Findlay, A. Beeby, T. B. Marder and S. Umapathy, *ChemPhotoChem*, 2022, **6**, e202200146.
50 F. Xu, K. Gong, W. Fan, D. Liu, W. Li, L. Wang and X. Zhou, *ACS Appl. Energy Mater.*, 2022, **5**, 13780.
51 X. Liu, Z. Xu and J. M. Cole, *J. Phys. Chem. C*, 2013, **117**, 16584.
52 Y. Zhou, Y. Xiao, S. Chi and X. Qian, *Org. Lett.*, 2008, **10**, 633.
53 F. Bures, W. B. Schweizer, J. C. May, C. Boudon, J.-P. Gisselbrecht, M. Gross, I. Biaggio and F. Diederich, *Chem. – Eur. J.*, 2007, **13**, 5378.
54 H. K. J. Snaith, L. Schmidt-Mende, M. Grätzel and M. Chiesa, *Phys. Rev. B:Condens. Matter Mater. Phys.*, 2006, **74**, 045306.
55 K. J. Moon, S. W. Lee, Y. H. Lee, J. H. Kim, J. Y. Ahn, S. J. Lee, D. W. Lee and S. H. Kim, *Nanoscale Res. Lett.*, 2013, **8**, 283.
56 M. C. Tsai, Y. C. Chiu, M. D. Lu, Y. L. Tung, H. C. Tsai, J. R. Chang Chien and C. Y. Lin, *ACS Appl. Energy Mater.*, 2020, **3**, 2744.

